Hindawi
Shock and Vibration
Volume 2024, Article ID 3388056, 14 pages
https://doi.org/10.1155/2024/3388056

Research Article

Simulation of Transient Temperature and Clearance after Shutdown of Aeroengine Based on CFD and FEA Coupled Models

Xuanming Ge, Yan Gao, Wei Gu, Dongyu Sui, and Lingling Yue

AECC Commercial Aircraft Engine Co.,LTD., Shanghai 201100, China

Correspondence should be addressed to Xuanming Ge; andygxm@163.com

Received 24 January 2024; Revised 2 March 2024; Accepted 21 March 2024; Published 8 April 2024

Academic Editor: Jiaqiang E.

It is crucial to comprehend the heat soak phenomenon, which may result in a significant temperature increase after the shutdown followed by a gradual decrease. This could bring potential risks for the engine including oil coking. The temperature change of engine components dictates the clearance after shutdown, while startup strategies are primarily based on this. A simulation strategy, utilizing computational fluid dynamics (CFD) and finite element analysis (FEA) coupled models, is suggested to investigate the transient temperature and clearance after shutdown. The maximum temperature deviation between the simulation result and experimental data are less than 6%. Flow parameters, including velocity and mass flow rate obtained from the CFD result, were applied as boundaries of the FEA model. Based on the FEA model, transient temperature calculations were also conducted for 20 hours after shutdown. The results indicate that the FEA model demonstrates good agreement with the CFD simulation, with a maximum deviation of less than 5% and at only 0.2% of the simulation time. After the engine shuts down, the stator's temperature change rate is faster than that of the rotor due to better cooling conditions and relatively small heat capacity. Consequently, the seal clearance increases in the initial period after shutdown and then decreases to a minimum value. The nondimensional minimum clearance can be 0.8 times the cold state value at the location of the high-pressure turbine seal.

1. Introduction

The flow patterns within the engine dictate the heat transfer intensity, subsequently impacting the temperature distribution of the engine components. As a result, studying the fluid flow patterns within the engine is crucial, with computational fluid dynamics (CFD) being the predominant method. Researchers have conducted studies at both component and whole engine levels. Negulescu and Pfitzner developed a system using tubeless vortex reducers to achieve deswirl via the CFD method [1]. By using CFD tools, the model with tubeless vortex reducer shows an increase in the relative swirl from 0.85 to 1.4 at the entry of nozzles of the vortex reducer which has a good agreement with the test data. Aidarinis and others used CFD to analyze airflow in the aeroengine front-bearing chamber [2]. Che and others utilized CFD for the whole engine basin simulation [3], after a more detailed analysis of the fluid, and due to the cavity effect, the actual thrust of the entire engine is significantly reduced by up to 30%, and the specific fuel consumption (SFC) is noticeably increased, with a maximum increase of up to 55%. Conan and Savarese [4] and Innocenti et al. [5] applied CFD to assess bleed airflow in the aeroengine. Yan and others employed the CFD unsteady method to simulate the inlet temperature distribution of the turbine [6], and the unsteady simulation using CFD has been effectively utilized to capture the flow pattern in the turbine stage. It was predicted that in the presence of hotspots at the turbine inlet, the highest temperature nonuniformity along the radial direction increased by 0.02 on the vane and 0.05 on the blade. Otter and others used CFD for aeroengine exhaust system simulation [7]. Research has shown that the error between the thrust coefficient, bypass discharge coefficient, and core discharge coefficient obtained from the three-dimensional CFD method and the experimental data is only 0.03%, 0.37%, and 0.31%, which fully demonstrates the accuracy of the CFD method. Chen and others conducted numerical simulations on the entire aeroengine, employing

the CFD time-marching through-flow method to analyze the engine's flow field and performance [8] and research shows the CFD result and experimental deviations of the entire engine are not greater than 7%, which meets the accuracy requirements for engineering applications. Zhang and others predicted the compressor stage characteristics via 3D CFD numerical simulations, achieving surge boundary prediction and stability expansion of multistage compressors [9]. Sun and others simulated the three-dimensional flow in the vortex cavity, as well as the temperature field and stress distribution of the turbine disc using CFD [10]. Sun and others utilized CFD and FEA coupling methods to study the engine's secondary air system [11]. The completion of the thesis involved the coupled calculation of the CFD-FEA model focusing on the low-pressure turbine disk cavity. The author believes that the FEA method is a practical engineering approach with a high efficiency and accuracy. However, FEA results are dependent on a large database and engineering experience. The CFD-FEA coupled method is currently a costly analysis tool, but it fully utilizes the accurate flow solutions of CFD and the temperature and stress results characteristics of FEA. It remains a promising direction for the future. Illingworth and others performed three-dimensional flow heat transfer coupling simulations on the engine's preswirl system, analyzing the flow and heat transfer conditions under maximum take-off conditions [12]. This article presents a coupling code developed based on Fluent software, and applies it to the preswirl system of the Trent 500 model. With the help of the code, the two-dimensional axisymmetric CFD model coupling, and the three-dimensional CFD model coupling took 34 hours, and 14 days, respectively. Although the coupling time is still relatively long, the precision gains brought by the CFD-FEA coupling model are still very appealing.

Finite element analysis (FEA) is a technique used to determine the degrees of freedom (DOF) by breaking down solid objects into multiple small elements and then evaluating the DOF of each element through interpolation. Numerous simulations of temperature, stress, and deformation of aeroengine components have been carried out by scholars using the FEA method. For instance, Qu et al. undertook a simulation analysis of the mechanical properties of the engine main bearing under high-temperature conditions and provided a life analysis of the main bearing [13] and based on the simulation results, the stress in the contact area of the bearing's steel ball is approximately 28 times that of the stress in other noncontact areas. Jinhua et al. performed a temperature field simulation of a turbine disc based on the FEA method and compared the impact of coupling the temperature field with the air system on the calculation result [14]. And it has been demonstrated that fluid thermal calculation method has enhanced the accuracy of simulation. Compared to the uncoupled calculation results, the maximum error of the coupled calculation results with experimental data has been reduced by 10 K. Cao and Han conducted a thermal-solid coupling simulation based on the FEA method for the turbine disc and blade to obtain actual clearance values of the high-pressure turbine blade tip at the front edge and rear edge, guiding the structural design of the high-pressure turbine [15], and based on the detailed simulation FEA calculation of the heat transfer and deformation coupling model, it is found that the blade of a certain engine should ensure a cutting angle of 19.77′ to maintain a uniform clearance value at the leading and trailing edges of the blade under thermal conditions. Juethner et al. utilized a FEA model to simulate the thermal bending of the rotor under operational conditions [16]. Sun et al. combined finite element analysis with computational fluid dynamics (CFD) to complete temperature field simulation of rotor parts [17]. This study proposes a coupling acceleration algorithm for the CFD-FEA coupling method. This method treats the heat transfer process as a transient process and computes the CFD model and exchanges data at certain time points throughout the transient history. This approach accelerated the simulation by 1.4 and 3.1 times in two test cases, respectively. This method also provides significant inspiration for the simulation in this study. Papanikos et al. carried out stress and deformation analysis and calculations based on the three-dimensional finite element simulation for the dovetail connection position of the engine rotor disc [18].

Based on a review of the literature, extensive simulations and analyses of engine performance under operating conditions have been conducted using FEA or CFD methods. However, research on fluid flow and heat transfer after the engine shuts down is limited. Only a small number of studies exist, such as Shaojie's et al. simulation of the natural cooling process of a rotating disc cavity after shutdown based on a 2D axisymmetric model [19]. It is important to note that due to limitations of the model, the true thermal conduction process and circumferential nonuniformity of airflow after shutdown are not fully reflected. Shuguang et al. analyzed and determined the location of a low-pressure turbine block based on a measured clearance value [20] and the survey points out that the engine was found at the #5 bearing, with a radial clearance smaller than the designated minimum value of 0.1 mm, resulting in the rubbing. Kanike et al. used a finite element model in Ansys to simulate and predict temperature for analyzing the heat soak phenomenon at the bearing location after shutdown [21].

It is crucial to analyze the fluid flow and heat transfer following shutdown for several reasons. Once the engine is shutdown, efficient cooling flow within the engine ceases, potentially causing the temperature of components to exceed those during operation due to the heat soak phenomenon. This poses a greater risk to the engine's internal components after shutdown than during operation. In addition, the transient clearance of seals during natural cooling following shutdown is essential, as startup strategies heavily rely on it to facilitate quick restarts without stator-rotor rubbing. Furthermore, the flow and heat transfer dynamics after shutdown differ significantly from those under operating conditions, warranting an in-depth study based on a comprehensive engine model.

This article introduces a comprehensive fluid-solid coupling CFD model primarily utilized for examining the flow characteristics of fluid inside the engine after shutdown. It also presents a 2D finite element model for calculating the

transient temperature and seal clearance values during the natural cooling process to enhance simulation efficiency. Using these two models, the article proposes a coupling simulation strategy to improve simulation accuracy by incorporating flow parameters such as the mass flow rate in the main flow channel and in the secondary air system cavities as boundaries for the finite element model. This strategy not only leverages the efficiency of 2D FEA models but also ensures high accuracy, as the CFD model offers reliable flow patterns. The schematic diagram of the CFD-FEA coupling strategy is shown in Figure 1.

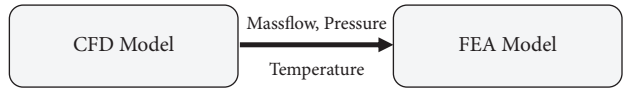

Figure 1: Schematic diagram of the CFD-FEA coupled method.

2. Simulation Models

2.1. CFD Model and Validation. A reliable fluid flow simulation is essential to accurately simulate the postshutdown engine temperature. The temperature of engine components greatly influences the surrounding airflow, resulting in an uneven distribution of air temperature. As hot air rises and cold air sinks, a temperature distribution is gradually formed, with upper components being hot and lower components being cold. Therefore, a fluid-solid coupling model is indispensable to capture the intense interaction between the fluid and solid components.

To guarantee the legitimacy of the model, this article constructs a 3D solid domain and 3D fluid domain in the CFD model, as depicted in Figure 2. The solid domain encompasses the entirety of engine components such as the fan, boost stage, ten-stage high-pressure compressor and blades, two-stage high-pressure turbine and blades, seven-stage low-pressure turbine and blades, core module cover, and nozzle. The fluid domain encompasses the fluid within the main flow channel, the fluid within the secondary cavity, and the ambient environment outside the engine. The model has been simplified to a certain extent, such as the transformation of the seal structure into a narrow slit, the simplification of blades into flat plates, and the omission of internal structures such as air ducts and accessories inside the core module cover. The bearing now only includes the outer surface of the oil cavity, disregarding internal details. The thermal contact resistance between components is not considered, and the heat is fully conducted between the adjacent components.

The given partial view of solid and fluid meshes are shown in Figures 3 and 4, as it is not easy to identify the entire grid. The solid domain grid consists of 24.08 million elements, while the fluid domain grid comprises 347 million elements. The simulation is performed using CFX software and the convergence criterion is set to an RMS value of $1e-7$. The natural cooling process of the engine after shutdown is a highly complex process, with flow at different locations and different times that may be turbulent or laminar. This article assumes turbulent flow and uses the SST turbulence model for solving the process. Subsequently, in the FEA model, the heat transfer coefficient is set to match the simulated temperature values with the experimental values, thereby reducing the impact of flow uncertainty.

The open boundary type is set for the outer cylindrical surface of the fluid domain, with reference pressure set to 0 Pa and operating temperature set to 293.15 K. The other

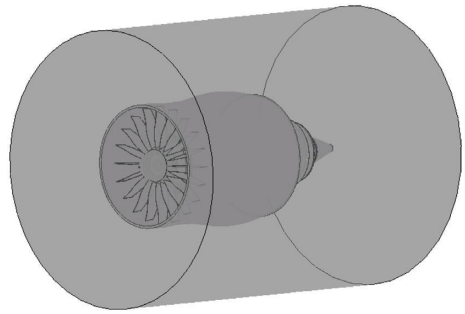

Figure 2: Schematic diagram of the engine model.

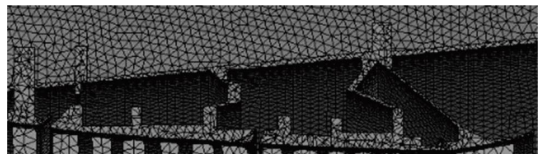

Figure 3: Partial view of mesh in the solid domain.

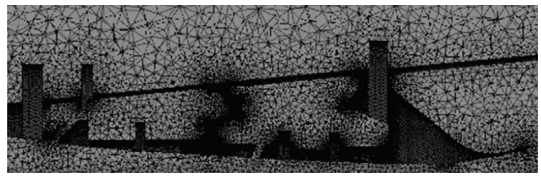

Figure 4: Partial view of mesh in the fluid domain.

surface of the fluid domain is set to solid-fluid interface boundary type, which can be explained by equation (1). The normal component of heat flux q can be calculated by static temperature gradient ∇T of fluid and λ_{fluid} is the thermal conductivity of the fluid. This heat flux is the same as the flux at the boundary of the solid domain which can be determined by the heat transfer coefficient h and the difference between local reference temperature and solid temperature.Also, h is determined by the CFX solver which has no effect on the accuracy of the solution.

$$\frac{\lambda_{\text{fluid}} \nabla T \cdot \mathbf{n}}{|\mathbf{n}|} = h\left(T_{\text{ref}} - T_{\text{solid}}\right). \tag{1}$$

After shutdown, the fluid pattern can be predominantly characterized by a radial natural cooling flow driven by temperature differentials, which are largely separate from each cavity. Under operating conditions, the airflow is typically driven by shear force, Coriolis force, and other factors. The cooling air from the compressor exchanges heat with the solid surface through forced convection through holes and labyrinth seals, ultimately reaching the main flow channel. Using the 5^{th} disc cavity of the compressor as an example, a comparison of natural convection flow and

operating condition flow is shown in Figures 5 and 6. The scales in the figures represent the nondimensional flow velocity in the disc cavity as V_{nd}. The definition of V_{nd} is provided in equation (2), where V_{loc} denotes the local flow velocity, and V_{max} represents the maximum flow velocity on the section plane.

$$V_{nd} = \frac{V_{loc}}{V_{max}}. \tag{2}$$

The simulation object of this article is a certain engine. Thermocouples 1–3 are positioned on the outer casing of the high-pressure compressor entraining cavity, while thermocouples 4 and 5 are situated on the outer casing of the interstage load-bearing frame and the rear sealing structure. Thermocouple 6 is located near the #5 bearing' outer surface, specifically on the labyrinth seal. These thermocouples are used to verify the accuracy of the CFD model by comparing the test data with the simulation results, following a six-hour data acquisition period postengine shutdown after a running test.

The CFD model's accuracy is depicted in Figure 7. The temperature difference is represented by equation (3). For each thermocouple, the maximum difference is less than 6%. T_{CFD} and T_{EXP} represent simulation temperature results and test data. All temperature units are in Kelvin.

$$T_{diff} = \frac{T_{CFD} - T_{EXP}}{T_{EXP}} \times 100\%. \tag{3}$$

The difference may be attributed to the simplification of structures, including accessories and the active clearance control system entraining tube in the core module. This simplification could influence the airflow pattern and in turn impact the temperature of the outer casing. In addition, the initial temperature distribution of the CFD model might not perfectly align with the real engine. Nevertheless, it is estimated that this difference will have a maximum impact on deformation of not more than 0.2 mm. This level of accuracy in the interested seal clearance meets the requirements for simulation. Hence, the CFD model demonstrates sufficient accuracy and precision for simulating flow and heat transfer after shutdown.

2.2. FEA Thermal Model of Whole Engine. Based on high-performance simulation power, the 20-hour natural cooling simulation took almost 2 weeks. This method is not acceptable for structure design or optimization. To efficiently calculate the transient temperature and seal clearance, a 2D FEA thermal model was created using Ansys APDL, as shown in Figure 8. The model is meshed with axisymmetric elements, except for plane elements with thickness for discrete structures. The FEA model consists of 41769 elements, which is only 1% of the solid domain grid in the CFD model.

The flow path is designated as entering from the fan through the high-pressure compressor, high-pressure turbine, low-pressure turbine, and nozzle as depicted in Figure 8. According to the CFD result, an intriguing observation is that the fluid in the flow path forms two streams with opposite flow directions. Stream 1 initially flows from the combustor back to the compressor, while

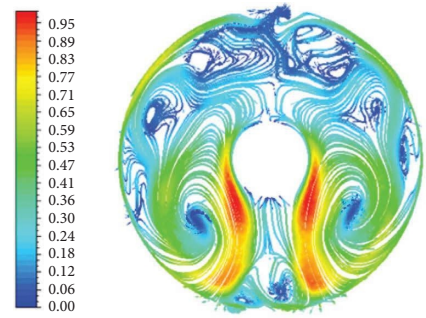

Figure 5: Natural cooling flow.

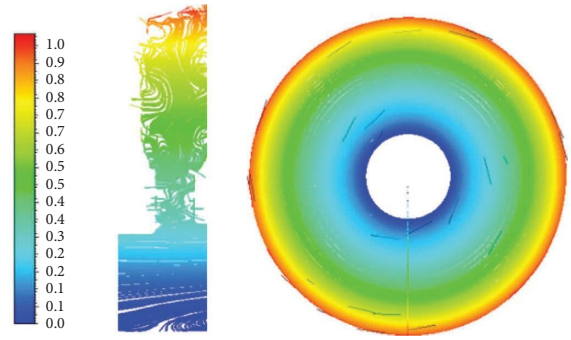

Figure 6: Flow under operating conditions (front view and left view).

stream 2 flows from the combustor to the nozzle through the turbine. The velocity vector is illustrated in Figures 9 and 10.

Consequently, a 1D fluid flow network is simulated in the flow path, starting from the combustor and flowing to both sides. The heat transfer coefficient is set between the streamline and the surface, as well as the flow rate and the inlet temperature of the network.

The other boundary type is a single-node thermal equilibrium cavity, also known as a thermal void. The thermal void assumes that there is sufficient heat exchange between the surrounding solid wall and the fluid node. This boundary should only be used where the fluid temperature is uniform. The thermal void boundary is used for all secondary flow cavities outside the main flow passage. For each thermal void boundary, the corresponding heat transfer coefficient is set.

The figure displays the schematic boundary diagram in Figure 11.

The concept of flow network boundary is described in equation (4), while the thermal void boundary is delineated in equation (5):

$$\left(T_f - T_{s,j}\right) \cdot \mathrm{HTC}_j \cdot A_j + Q_j = m_j \cdot c \cdot dT_f, \tag{4}$$

$$\sum_{j=1}^{n} \left(T_f - T_{s,j}\right) \cdot \mathrm{HTC}_j \cdot A_j = 0, \tag{5}$$

where T is the temperature K; HTC is the heat transfer coefficient $W/(m^2 \cdot K)$; A is the heat transfer area m^2; Q is the input power W; m is the mass flow rate kg/s; c is the heat capacity $J/(kg \cdot K)$; f is *fluid*; s stands for *solid*; and j represents node j of the finite element.

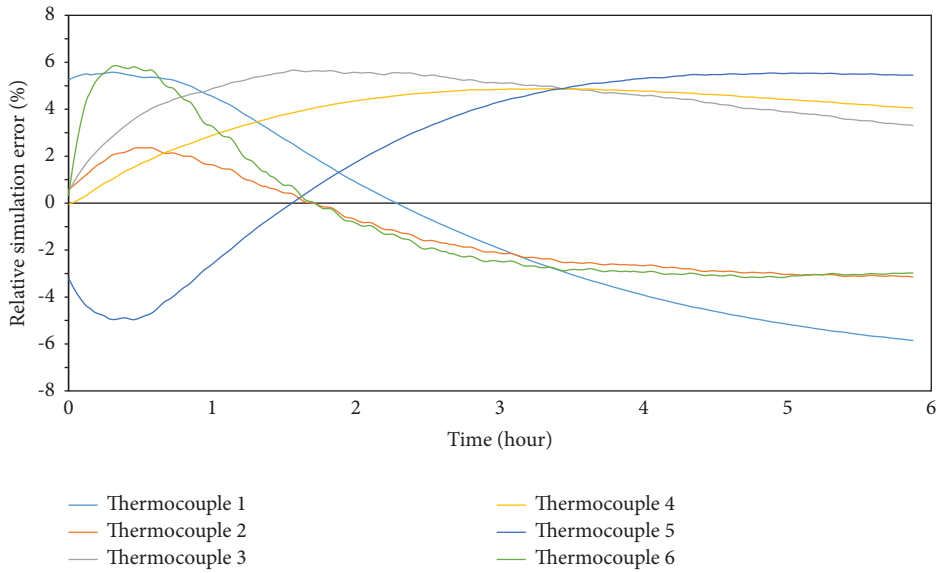

Figure 7: Difference between CFD simulation and test data.

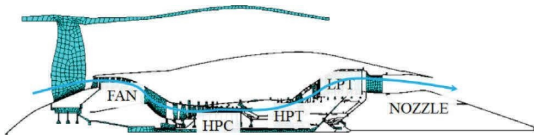

Figure 8: FEA model of the whole engine.

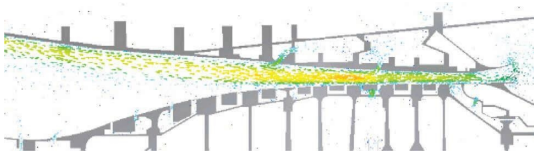

Figure 9: Direction of stream 1.

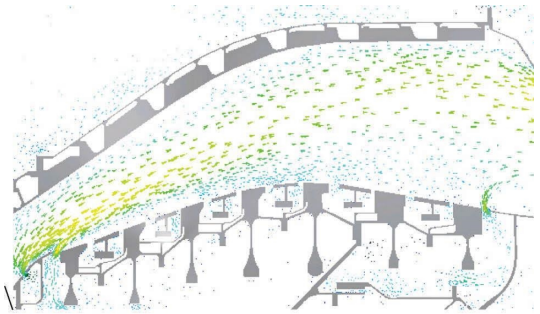

Figure 10: Direction of stream 2.

Surface elements in APDL were utilized to facilitate heat transfer between the fluid and solid. In addition, appropriate heat transfer coefficients (HTCs) need to be applied. Based on the results from CFD and previous experience, HTCs are typically categorized into four types: the first type pertains to the core module, the second relates to entraining cavities, the third is associated with the flow path, and the fourth is linked

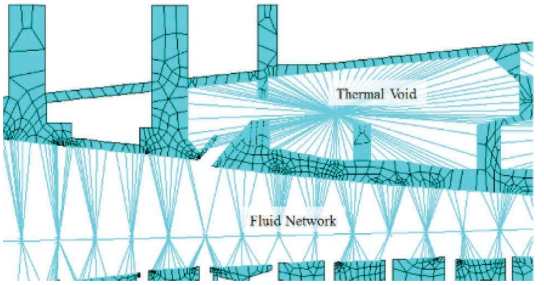

Figure 11: Schematic diagram of the boundary of the FEA model.

to disc cavities. Specifically, each type of HTC after shutdown represents 12.5%, 0.2%, 1%, and 1.25% of the value of the ground idle condition.

3. Simulation Results and Analysis

3.1. Results of CFD Simulation. A 20-hour natural cooling simulation was conducted after the engine shutdown, based on a CFD model. Typically, the actual engine shutdown process can be divided into two stages: the rotor speed gradually decreasing to 0 rpm in the first stage and a complete stop in the second stage. In the first stage, in addition to natural convection, there may be a certain forced convection due to rotor speed. To simplify the simulation, this study only focuses on the second stage. The temperature distribution under the ground idle condition is used as the initial field of the solid domain, while the initial temperature of the fluid domain is solved by the CFX steady solution, as shown in Figure 12. The nondimensional temperature T_{nd} is determined using equation (6), where T_{loc} represents the local temperature and T_{max} represents the maximum temperature of the initial field.

$$T_{nd} = \frac{T_{loc}}{T_{max}}. \quad (6)$$

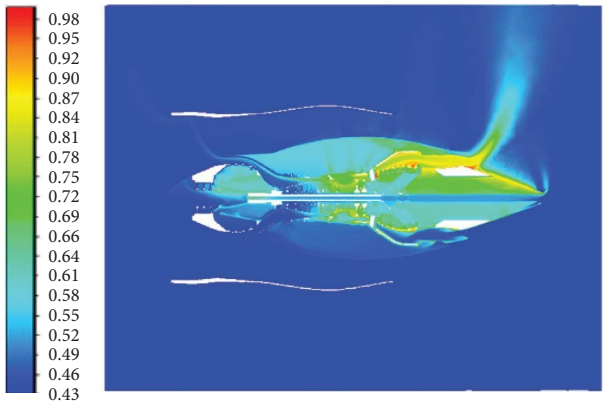

Figure 12: Initial temperature of the fluid domain.

As depicted in Figure 12, the air temperature distribution within the core module exhibits noticeable unevenness. The upward movement of hot fluid leads to the formation of a hot air trend at the top and cold air at the bottom, which proves challenging to replicate using the 2D simulation model.

Equation (7) is utilized for determining the nonuniformity of the circumferential air temperature in the core module, denoted as θ. Here, T_{max} and T_{min} represent the highest and lowest circumferential temperatures of a specific section and $\overline{T}$ denotes the average value. For instance, considering the temperature of the core module near the casing corresponding to the fifth-stage outer ring of the low-pressure turbine, the nonuniformity during downtime is 26%, while the maximum is 31% during the natural cooling process, as depicted in Figure 13.

$$\theta = \frac{T_{max} - T_{min}}{\overline{T}} \times 100\%. \tag{7}$$

After the shutdown, there is still some airflow through the main flow path. The velocity reaches its maximum at the outlet of the nozzle. The contour of the initial velocity is depicted in Figure 14. The maximum velocity in the flow path is approximately 1.9 m/s, while the velocity in the secondary air cavity is generally less than 0.1 m/s. Therefore, the temperature change of the fluid in the flow path is much more pronounced and cannot be disregarded while the temperature of the fluid in the secondary air cavity is relatively uniform.

3.2. Results of the FEA Model. In order to assess the consistency between the FEA model and the CFD model, we compare the initial temperature field of the solid.

The deviation between the FEA result and the CFD result is demonstrated at specific locations. As depicted in Figure 15, the deviation at each location is below 2%.

The initial fluid temperature field also impacts the transient temperature of the component after shutdown. As indicated in Table 1, the CFD result column depicts the average fluid temperature at a specific section. The FEA result represents the fluid temperature from the results of the 1D flow network in the FEA model, and all temperature values have been nondimensionalized. The maximum deviation is less than 5%. Hence, the temperature of the main flow fluid based on the FEA model also aligns well with the CFD result.

The temperature distribution of the HPC (high-pressure compressor) inlet section is depicted in Figure 16. The fluid with a relatively high temperature accumulates at the high-radius location, while the cold fluid accumulates at the low-radius location. However, based on the CFD result, the axial velocity in the flow path is primarily influenced by the high-temperature fluid. As a result, the fluid temperature in the 1D flow network closely aligns with the temperature of the high-radius airflow rather than the average value. This is the reason why maximum deviation occurs at the inlet section of the HPC.

During the natural cooling process, the engine typically experiences its highest and lowest circumferential temperatures at the 12 o'clock and 6 o'clock directions. To address this issue, the article conducts a simulation to depict the temperature distribution in the 12 o'clock direction, which signifies the highest temperature of the engine.

The FEA model was utilized to compute transient temperature over a span of 20 hours following engine shutdown. The FEA calculation results at specific locations were chosen for comparison with the CFD simulation results, in order to validate the FEA model.

The deviation in simulation between the FEA result and CFD result, T_{dev}, is calculated using equation (8). T_{FEA} represents the temperature result of the FEA model, and T_{CFD} stands for the temperature result of the CFD model. Based on the locations where thermocouples 1–6 are installed, as mentioned in Section 2.1, a comparison of the temperature calculation results of FEA and CFD is shown in Figure 17. The maximum value of deviation is less than 5%. The difference is primarily caused by the limitations of the 2D FEA model, which is incapable of simulating the circumferential distribution of fluid. In addition, the FEA model is unable to simulate the circumferential heat conduction.

$$T_{dev} = \frac{T_{FEA} - T_{CFD}}{T_{CFD}} \times 100\%. \tag{8}$$

To provide a more detailed comparison between the FEA model and the CFD model, we carried out additional comparisons at different locations. Figure 18 illustrates the schematic diagram of the honeycomb (referred to as location 1) and the labyrinth seal at the rear of the second stage disc of the high-pressure turbine (location 2).

The temperature deviation between location 1 and location 2 in the FEA and CFD models is depicted in Figure 19. The maximum deviation is approximately around 3.5% half an hour after shutdown.

The temperature variation in the outer casing of the 4^{th} stage (location 3) and 7^{th} stage (location 4) entraining cavity as well as the outer casing of the interstage load-bearing frame (location 5) are illustrated in Figure 19. The variation curves from location 6 to location 7 are displayed in Figure 20. The results indicate that constant HTC in the FEA model slightly overestimated the natural cooling effect after

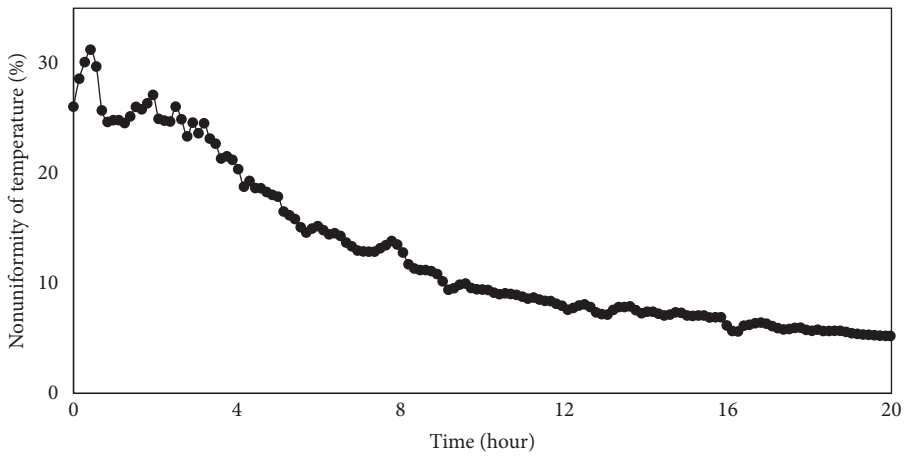

Figure 13: Air temperature nonuniformity in the core module.

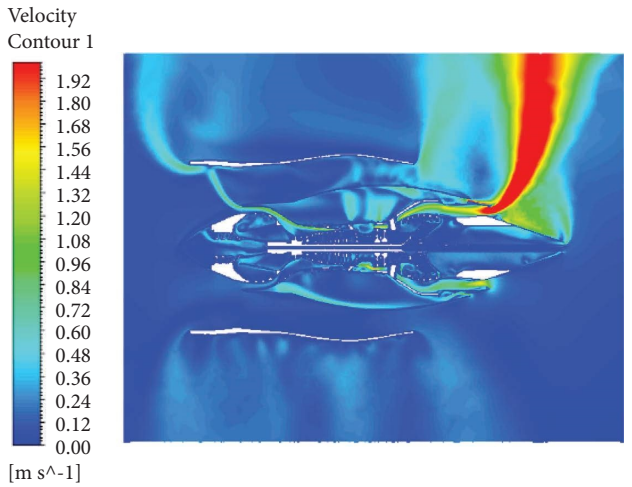

Figure 14: Velocity of the fluid domain (time = 0).

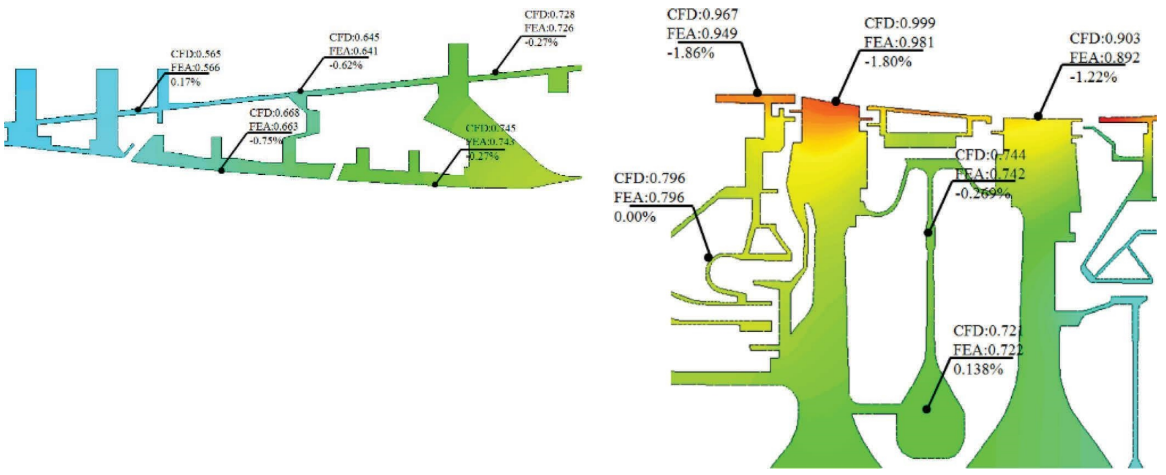

(a) (b)

Figure 15: Comparison of temperature between CFD and FEA results (time = 0). (a) Compressor casing. (b) High-pressure turbine rotor.

Table 1: Comparison of initial fluid temperature.

Section location	CFD result	FEA result	Deviation (%)
Inlet of HPC	0.510	0.486	−4.70
Outlet of HPC	0.754	0.734	−2.70
Inlet of HPT	0.733	0.727	−0.82
Inlet of LPT	0.754	0.752	0.27
Outlet of LPT	0.828	0.834	0.72

HPT, high-pressure turbine; LPT, low-pressure turbine; HCP, high-pressure compressor.

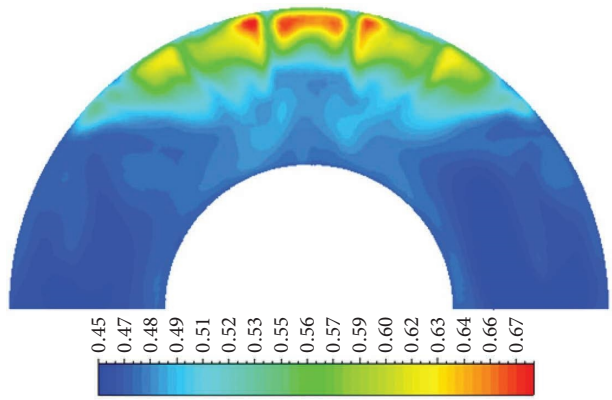

Figure 16: Temperature distribution at HPC inlet section.

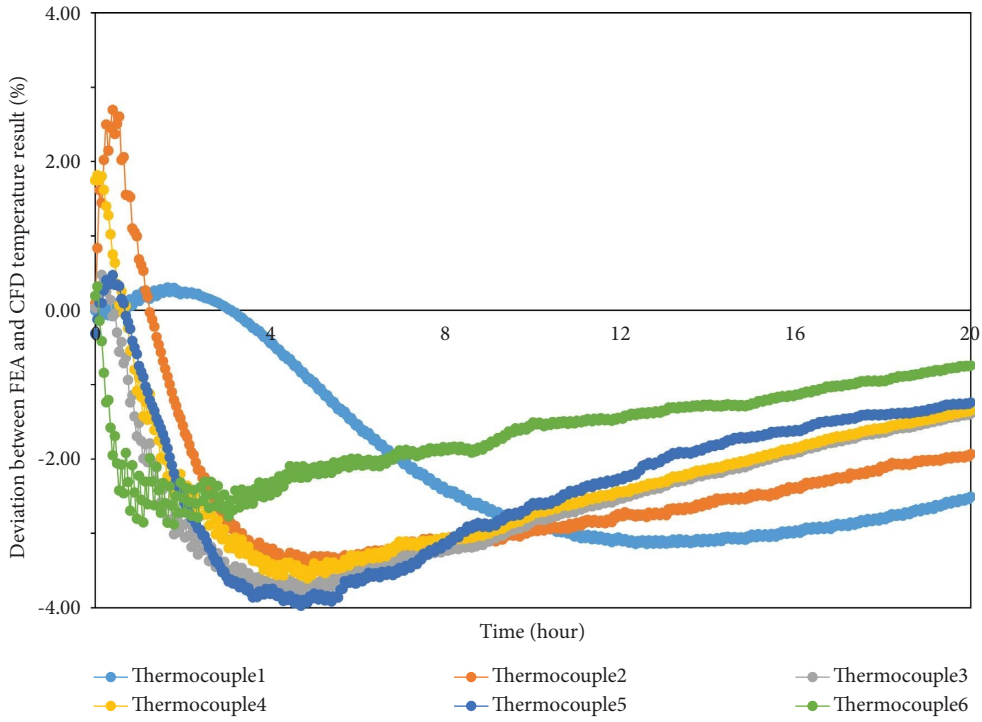

Figure 17: Deviation between FEA and CFD results at the locations of 1–6 thermocouples.

shutdown due to the gradual increase in temperature difference, resulting in positive deviation. Subsequently, as the temperature difference decreases gradually, the deviation becomes negative. The maximum deviation is less than 5.8%.

The temperature difference between the compressor's 5th disc bottom (position 6) and the labyrinth disc bottom (position 7) is illustrated in Figure 21. The maximum deviation is still less than 5%.

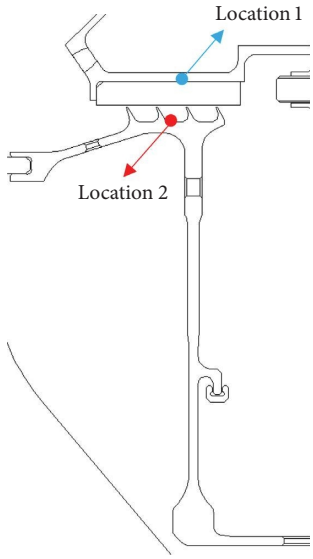

Figure 18: Schematic diagram of locations 1 and 2.

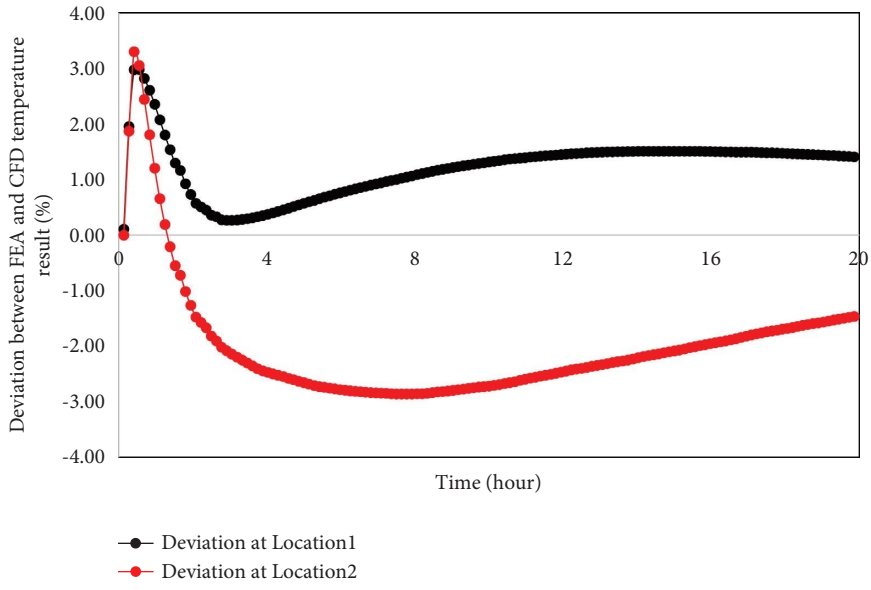

Figure 19: Deviation of temperature of locations 1 and 2.

In general, the maximum deviation between the transient calculation results of the FEA model and the temperature results of the CFD model simulation is less than 6% at locations 1 to 7. Therefore, the FEA result demonstrates a strong agreement with the CFD temperature result. In comparison to developing a solid domain model in CFD, the FEA model offers significant computational cost savings with only 1% of the grid quantity and merely 0.2% of the computational time. For the specified engine, the fluid network and thermal void boundary with appropriate HTC as discussed in Section 2.2 can be a common method for transient temperature after shutdown. Hence, the subsequent analysis of the clearance changes after the shutdown will be conducted based on the FEA model.

3.3. Result of Temperature Simulation and Clearance Calculation after Shutdown. After the engine is shutdown, the temperature of parts near the main flow channel decreases rapidly, and the heat is gradually conducted from the disc rim and outer ring to the low-radius and low-temperature locations inside the engine, such as the bore of the disc and bearing. This is known as the heat soak phenomenon. Due to the effect of heat conduction, the temperature of those locations will gradually start to rise, and it can even exceed the temperature at the time of shutdown, before decreasing back to the ambient temperature. Taking the 6th stage of the compressor's rotor disc and the compressor discharge pressure (CDP) labyrinth disc as examples, the temperature curves of the rim and bore after shutdown are depicted in Figure 22. The

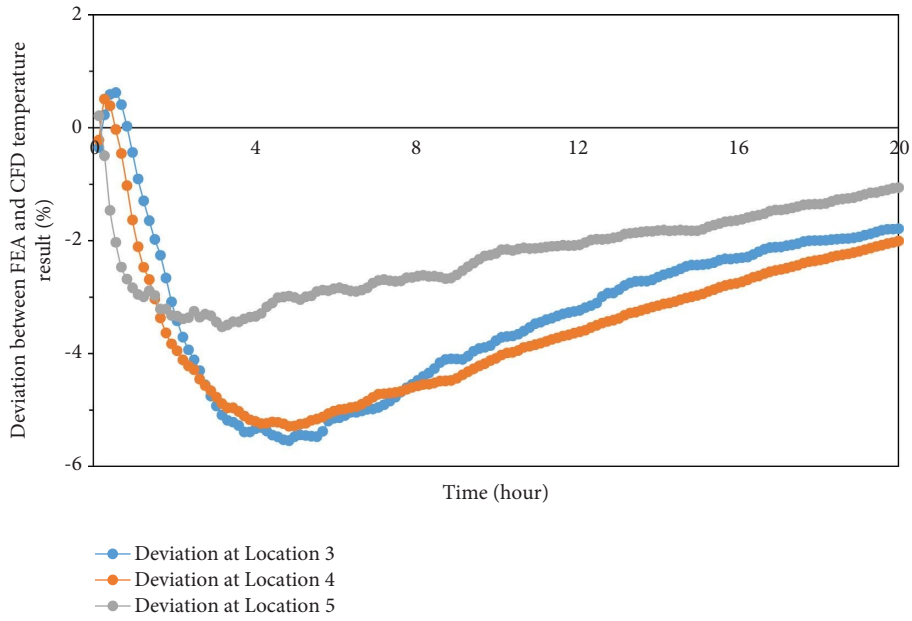

Figure 20: Deviation of temperature of locations 3, 4, and 5.

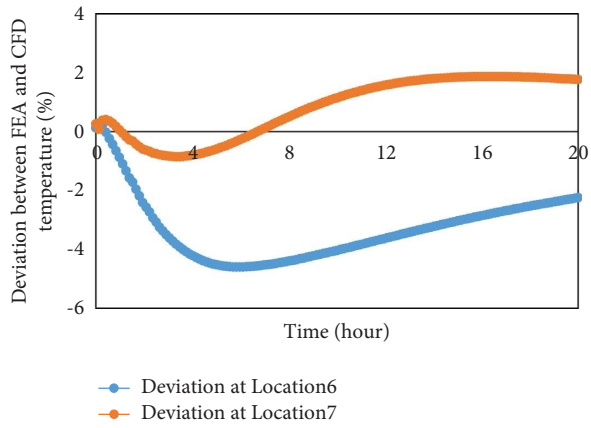

Figure 21: Deviation of temperature of locations 6 and 7.

temperature of the 6th disc bore rises from 0.504 to 0.557 in 1.3 hours, and the temperature of the CDP labyrinth disc bore rises from 0.694 to 0.732 in 0.7 hours. Meanwhile, the temperature of both disc rims decreases rapidly after shutdown, as the heat has been conducted to lower-temperature components such as bores and bearings within the engine.

Similarly, the outer surface temperature of bearing #4 gradually increases under the effect of heat soak, as depicted in Figure 23. It reaches its peak value approximately four hours after shutdown. Consequently, this increase in temperature could potentially lead to oil coking if not addressed promptly.

Due to insufficient cooling airflow, the temperature of the casing also increases initially. The transient temperature curves of the casing are illustrated in Figure 24, with the peak temperature being reached within just 50 minutes. The temperature at this time point imposes a more rigorous condition for core module accessories.

The stator's temperature typically decreases faster than the rotor's after reaching its peak, leading to a gradual reduction in sealing clearance, which may even fall below the design requirement. Without a comprehensive analysis of the clearance change after shutdown, there is a significant risk of rotor-stator rubbing during the hot startup.

Taking the seal between location 1 and location 2 as an example, the transient temperature after shutdown is illustrated in Figure 25: the temperature of location 1 rises from 0.63 to 0.68, and the temperature of location 2 rises from 0.63 to 0.70 due to heat soak. Subsequently, as natural cooling progresses, the temperature of components decreases. The temperature change rate on the stator exceeds that on the rotor, whether it rises or drops.

The nondimensional transient clearance between positions 1 and 2 is depicted in Figure 26. With the stator's much higher temperature, the clearance gradually increases to its

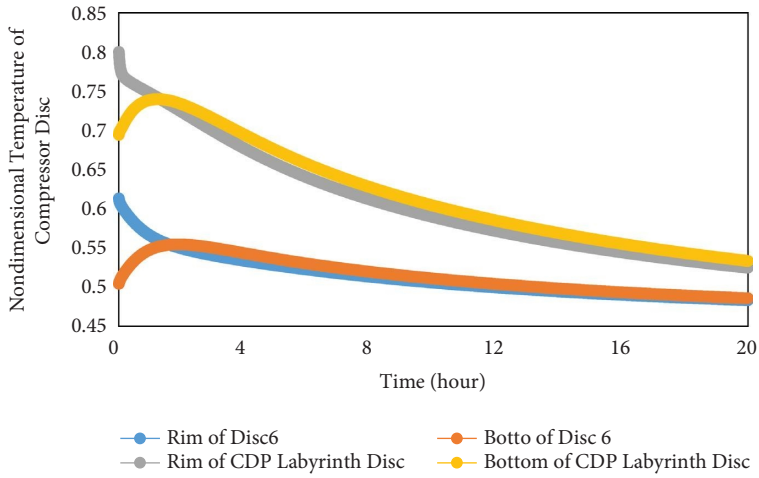

Figure 22: Nondimensional transient temperature of HPC discs.

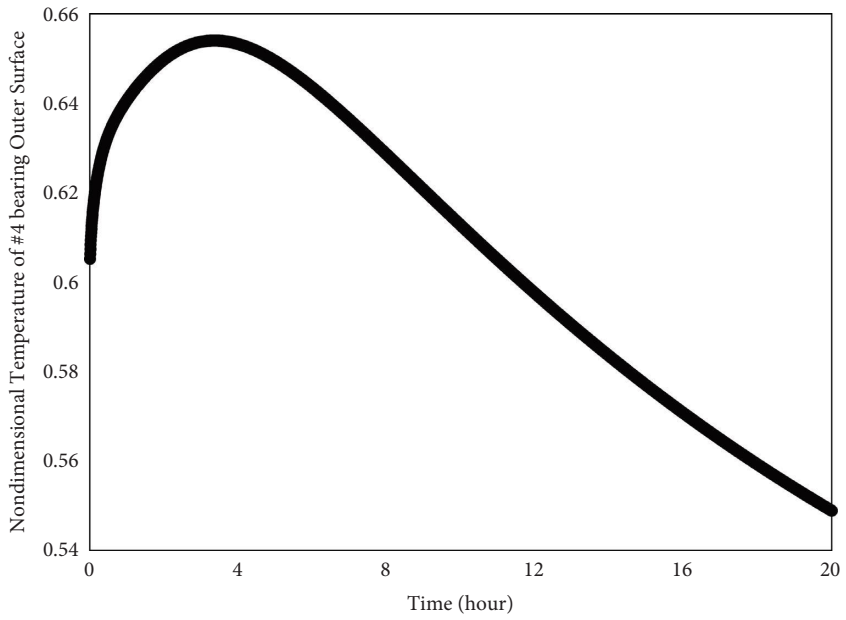

Figure 23: Nondimensional transient temperature of #4 bearing outer surface.

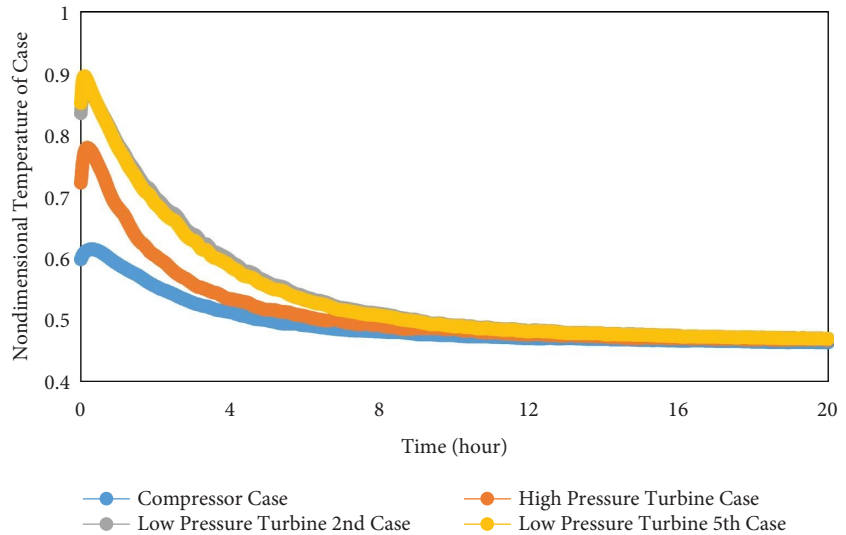

Figure 24: Nondimensional transient temperature of the case.

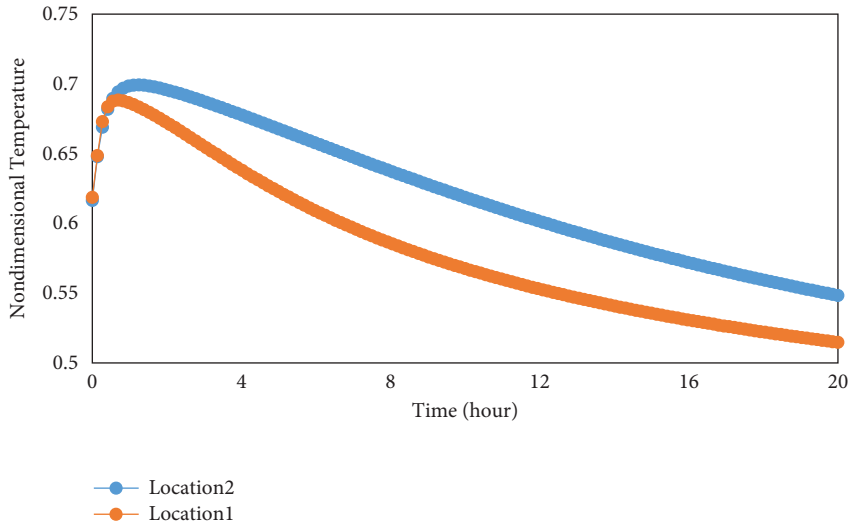

Figure 25: Nondimensional transient temperature of locations 1 and 2.

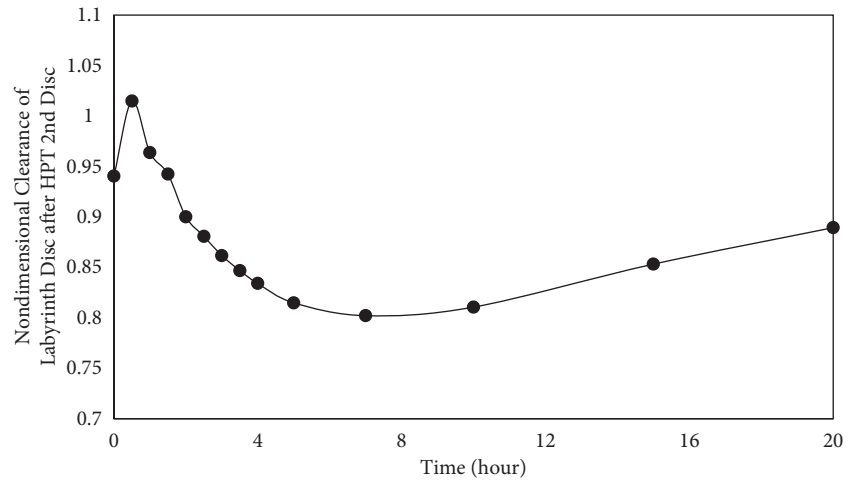

Figure 26: Nondimensional transient clearance of locations 1 and 2.

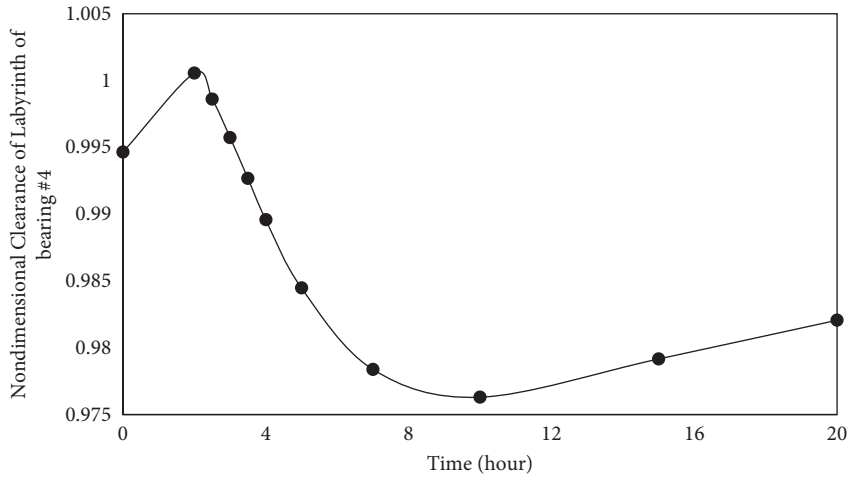

Figure 27: Nondimensional transient clearance of bearing #4 labyrinth.

Table 2: Comparison of CFD and FEA models.

	CFD	FEA
Cost	High	Low
Accuracy	High	High (only with appropriate boundaries)
Modification	Hard	Easy

maximum. Then, as the stator's temperature decreases much faster than that of the rotor, the clearance also decreases. A minimum clearance value is reached during the natural cooling process, posing the greatest risk for rapid hot startup. Nondimensional clearance C_{nd} is determined by dividing the transient clearance calculation value C_{loc} by the cold design value C_{cold} as illustrated in the following equation:

$$C_{nd} = \frac{C_{loc}}{C_{cold}}. \tag{9}$$

Another location susceptible to rotor-stator rubbing is the seal labyrinth of the #4 bearing. Its nondimensional transient clearance after shutdown is displayed in Figure 27. Similar to the trend in Figure 26, the clearance first increases, and then gradually decreases to a minimum value before returning to the cold state value.

It is clear that the labyrinth's clearance initially increases due to the stator's temperature rising more rapidly than the rotor's. Subsequently, with better cooling and a relatively smaller heat capacity, the stator also cools down faster than the rotor, causing the clearance to reach a minimum. After a sufficient period of time, the temperatures of the stator and rotor reach ambient temperature, and the clearance ultimately returns to the cold state value. It is worth noting that all the transient simulations in this article are based on the ground idle condition which is not that of a high temperature. If the engine shuts down from larger operating conditions, with much more intense natural convection, the seal clearance will change much more rapidly which brings greater risk for a hot startup.

4. Conclusions

This article has conducted a 20-hour natural cooling transient simulation using a fluid-solid coupling CFD model of a complete engine. A 2D FEA model has been created to efficiently simulate clearance. The main conclusions that can be drawn from this work are as follows:

(1) The CFD results effectively support the study of the heat soak phenomenon. The temperature deviation between the CFD model simulation and the thermocouple data is less than 6%, which can be attributed to a maximum of 0.2 mm deformation difference, occurring only in the case with the largest radius. This deviation has basically no impact on the clearance value for the interested seal labyrinth, which is typically located at a low radius. Therefore, the CFD model demonstrates sufficient accuracy in simulating conditions after engine shutdown.

(2) The 2D FEA model aligns well with the results from the CFD. It exhibits a relatively accurate maximum 6% temperature deviation compared to the CFD results. The FEA model can be used to simulate the transient temperature and labyrinth clearance after the engine shuts down. With only 1% of the elements compared to the solid domain in the CFD model, the FEA model saves almost 99.8% of simulation time, making it a more practical method in engineering. HTC after shutdown can be categorized into four types, and for the specific engine, each type of HTC can have specific proportions compared to that of the underground idle condition, as discussed in Section 2.2. To some extent, the FEA model can be run without the input of the CFD model, making it a common method for analyzing transient temperature and clearance after shutdown.

(3) The temperature of components near the main flow path decreases rapidly after shutdown, while the temperature of locations such as the disc bottom, bearing, and outer casing increases to a certain extent initially. The temperature of the compressor 6th disc bore rises from 0.504 to 0.557 in 1.3 hours, and the temperature of the CDP disc bore varies from 0.694 to 0.732 in only 0.7 hours. The temperature of the #4 bearing outer surfaces rises from 0.608 to 0.653. In addition, with the heat soak phenomenon, the temperature of the case also rises and reaches its peak value within only 50 minutes. The peak temperature after shutdown should be taken into consideration as a more stringent condition for those locations.

(4) The transient temperature change of components after the engine shuts down causes the clearance to initially increase before decreasing to a minimum. The nondimensional minimum clearance of locations 1 and 2 can be 0.8 times its cold state value, occurring approximately 7 hours after the engine shuts down. The nondimensional minimum clearance of the labyrinth seal of the #4 bearing is 0.976 about 10 hours after shutdown. It is crucial to develop a quick hot-startup strategy in order to avoid stator-rotor rubbing.

The CFD coupling method is an effective and fundamental approach for simulating the intense coupling of flow and heat transfer effects. However, when using a commercial solver, modifying the solver equations is challenging, and adjusting the model based on experimental data are even more difficult. In addition, CFD modeling typically requires significant time for meshing and solving. Moreover, CFD usually cannot provide support for testing the effectiveness of optimizations, since it involves unacceptable model-building work. On the other hand, an FEA model offers a cost-effective solution with a smaller mesh quantity and shorter solution times, making it easier to modify the model by adjusting input parameters such as HTC. Furthermore, it efficiently supports subsequent structural optimization. However, building an FEA

model requires prior knowledge of the flow pattern and characteristics, for which assistance from CFD is usually necessary.

To summarize and compare the CFD and FEA models, Table 2 outlines their individual strengths and weaknesses in several aspects as follows: cost of computation, accuracy of the model, and modification of the model.

Data Availability

The data underlying this article cannot be shared publicly due to commercial confidentiality requirements.

Conflicts of Interest

The authors declare that they have no conflicts of interest regarding the publication of this paper.

References

[1] D. Negulescu and M. Pfitzner, "Secondary air systems in aeroengines employing vortex reducers," in *Turbo Expo: Power for Land, Sea, and Air*, American Society of Mechanical Engineers, New Orleans, LA, USA, July 2001.

[2] J. Aidarinis, D. Missirlis, K. Yakinthos, and A. Goulas, "CFD modeling and LDA measurements for the air-flow in an aero engine front bearing chamber," *Journal of Engineering for Gas Turbines and Power*, vol. 133, 2011.

[3] W. Che, S. Ding, and C. Liu, "A modeling method on aircraft engine based on the Component Method of secondary air system," *Procedia Engineering*, vol. 80, pp. 258–271, 2014.

[4] F. Conan and S. Savarese, "Bleed airflow CFD modeling in aerodynamics simulations of jet engine compressors," in *Turbo Expo: Power for Land, Sea, and Air*, American Society of Mechanical Engineers, New Orleans, LA, USA, July 2001.

[5] A. Innocenti, A. Andreini, D. Bertini, B. Facchini, and M. Motta, "Turbulent flow-field effects in a hybrid CFD-CRN model for the prediction of NO and CO emissions in aero-engine combustors," *Fuel*, vol. 215, pp. 853–864, 2018.

[6] W. Yan, Q. Wang, J. Xie, and T. Xu, "Numerical simulation of unsteady flow in turbine stage considering inlet temperature distortion," *Journal of North University of China*, pp. 1–8, 2024.

[7] J. J. Otter, I. Goulos, D. G. MacManus, and M. Slaby, "Aerodynamic analysis of civil aeroengine exhaust systems using computational fluid dynamics," *Journal of Propulsion and Power*, vol. 34, no. 5, pp. 1152–1165, 2018.

[8] Y. Chen, W. Hu, J. Du, H. Zhang, and J. Yang, "Numerical simulation of flow through aeroengine components and complete engines," *Journal of Engineering and Thermophysics*, vol. 44, no. 04, pp. 894–902, 2023.

[9] T. Zhang, W. Chen, W. Qiao, X. Zhao, and Y. Zhang, "Research on aerodynamic stability prediction model of multi-stage compressor coupled with three-dimensional CFD," *Propulsion Technology*, vol. 44, no. 10, pp. 79–88, 2023.

[10] Y. Sun, D. Wang, and F. Yiyu, "Numerical simulation of flow-thermal-structural coupling characteristics of complex turbine disc cavities," *Equipment Manufacturing Technology*, no. 07, pp. 58–61+111, 2023.

[11] Z. Sun, J. W. Chew, and N. J. Hills, "Use of CFD for thermal coupling in aeroengine internal air systems applications," in *Fluid Machinery and Fluid Mechanics: 4th International Symposium (4th ISFMFE)*, pp. 399–404, Springer, Berlin Heidelberg, August 2009.

[12] J. B. Illingworth, N. J. Hills, and C. J. Barnes, "3D fluid–solid heat transfer coupling of an aero engine pre-swirl system," in *Turbo Expo: Power for Land, Sea, and Air*, vol. 47268, pp. 801–811, Reno, NV, USA, November 2005.

[13] C. Qu, W. Tang, and Z. Zhang, "Finite element analysis of mechanical properties of aeroengine main bearings at high temperatures," *Mechanical Engineering*, no. 08, pp. 4–6, 2023.

[14] L. Jinhua, W. Zhao, L. Xu, M. Zou, and J. Ma, "Coupled calculation and experimental verification of aeroengine air system and thermal analysis," *Gas Turbine Testing and Research*, vol. 32, no. 03, pp. 24–28+52, 2019.

[15] H. Cao and W. Han, "Thermo-mechanical coupled analysis of uneven tip clearance in aeroengine under hot state," *Mechanical Design*, vol. 36, no. 10, pp. 80–85, 2019.

[16] K. Juethner, T. Rose, J. S. Kumar et al., "Finite element analysis of bent rotors," *Journal of Engineering for Gas Turbines & Power*, vol. 145, no. 1, Article ID 011025, 2023.

[17] Z. Sun, J. W. Chew, N. J. Hills, K. N. Volkov, and C. J. Barnes, "Efficient finite element analysis/computational fluid dynamics thermal coupling for engineering applications," *Journal of Turbomachinery*, vol. 132, 2010.

[18] P. Papanikos, S. A. Meguid, and Z. Stjepanovic, "Three-dimensional nonlinear finite element analysis of dovetail joints in aeroengine discs," *Finite Elements in Analysis and Design*, vol. 29, no. 3-4, pp. 173–186, 1998.

[19] C. Shaojie, G. Wei, S. Dongyu, and L. Wang, "Natural cooling thermal analysis of the high pressure rotor of an aero-engine: a preliminary study," *Global Power and Propulsion*, 2017.

[20] L. Shuguang, K. Zhang, and B. Wang, "Analysis and research on the fault of low-pressure rotor stalling in a certain aero-engine," *Aeronautical Maintenance and Engineering*, no. 04, pp. 93–96, 2017.

[21] N. Kanike, D. Taluru, N. Krishna, and K. G. Gujar, "Thermal analysis of gas turbine bearing compartment during normal operation period," in *Gas Turbine India Conference*, vol. 45165, pp. 505–511, American Society of Mechanical Engineers, Maharashtra, India, July 2012.